Journal of Biomechanics ∎ (∎∎∎∎) ∎∎∎–∎∎∎

Contents lists available at ScienceDirect

Journal of Biomechanics

journal homepage: www.elsevier.com/locate/jbiomech
www.JBiomech.com

Short communication

The influence of downstream branching arteries on upstream haemodynamics

Lachlan J. Kelsey [a,b], Karol Miller [b,e], Paul E. Norman [a,c], Janet T. Powell [d], Barry J. Doyle [a,f,g,*]

[a] Vascular Engineering Laboratory, Harry Perkins Institute of Medical Research, Perth, Australia
[b] Intelligent Systems for Medicine Laboratory, School of Mechanical and Chemical Engineering, The University of Western Australia, Australia
[c] School of Surgery, The University of Western Australia, Australia
[d] Vascular Surgery Research Group, Imperial College London, UK
[e] Institute of Mechanics and Advanced Materials, Cardiff University, UK
[f] School of Mechanical and Chemical Engineering, The University of Western Australia, Australia
[g] Centre for Cardiovascular Science, The University of Edinburgh, UK

ARTICLE INFO

Article history:
Accepted 20 July 2016

Keywords:
Computational fluid dynamics
Wall shear stress
Iliac aneurysm

ABSTRACT

The accuracy and usefulness of computed flow data in an artery is dependent on the initial geometry, which is in turn dependent on image quality. Due to the resolution of the images, smaller branching arteries are often not captured with computed tomography (CT), and thus neglected in flow simulations. Here, we used a high-quality CT dataset of an isolated common iliac aneurysm, where multiple small branches of the internal iliac artery were evident. Simulations were performed both with and without these branches. Results show that the haemodynamics in the common iliac artery were very similar for both cases, with any observable differences isolated to the regions local to the small branching arteries. Therefore, accounting for small downstream arteries may not be vital to accurate computations of upstream flow.

1. Introduction

An aneurysm is a localised dilation of an artery which is life threatening when ruptured. Aneurysms of the common iliac artery (CIAA) are predominantly seen in association with an abdominal aortic aneurysm (AAA). For men aged over 65 years, the prevalence of an AAA is approximately 2% (Svensjö et al., 2011), and in 25% of these cases, co-existent aneurysms occur in one or both common iliac arteries and in 7% of these cases aneurysms also occur in the internal iliac arteries (Norman et al., 2003). With respect to CIAAs there is no strong evidence base for their management (Huang et al., 2008), and compared with the progress of computationally-aided assessment of AAA rupture risk (Doyle et al., 2009; Doyle et al., 2014a, 2014b; Gasser et al., 2010) and other cardiovascular disease (Blacher et al., 1999; Pijls et al., 1996; Tonino et al., 2009; Wilkinson et al., 1998), little has been done to improve our ability to assess the rupture risk of CIAA. Therefore, in the author's opinion, the computational-haemodynamics within iliac aneurysms is an understudied subject. Notably, as there are two common/internal/external iliac arteries, if there exists different levels of aneurysm burden in a set of contralateral arteries, there is an excellent opportunity to compare the haemodynamics (disease-indicators, and geometry factors) of either side. This type of comparison cannot be done when studying AAA, and henceforth we believe that further study of the haemodynamics in iliac aneurysms has the potential to improve the understanding of aneurysm growth and rupture.

Computational fluid dynamics (CFD) has emerged as a powerful and popular tool for the study of haemodynamics in cardiovascular disease (Steinman et al., 2013; Sun and Xu, 2014). With appropriate boundary conditions and model assumptions, CFD can be used to model the haemodynamic behaviour in any vessel of the body using patient-specific geometries, typically derived from computed tomography (CT). While a CT-slice thickness in the range of 1–3 mm is typical when imaging for aortic aneurysms or the larger arteries (Tendera et al., 2011), at this resolution minor arteries are often omitted from many computational-models of this region. This may be particularly relevant in any attempt to model the haemodynamics within the iliac artery region, given the large number of branches of the internal iliac artery supplying the

Abbreviations: CIAA, Common Iliac Artery Aneurysm; AAA, Abdominal Aortic Aneurysm; CT, Computed Tomography; WSS, Wall Shear Stress; SC, Supraceliac; GCI, Grid Convergence Index; TAWSS, Time-Averaged Wall Shear Stress; OSI, Oscillatory Shear Index

* Corresponding author at: Harry Perkins Institute for Medical Research, 6 Verdun Street, Nedlands, Perth, WA 6009, Australia. Tel.: +61 8 6151 1084.
E-mail address: Barry.Doyle@uwa.edu.au (B.J. Doyle).

http://dx.doi.org/10.1016/j.jbiomech.2016.07.023
0021-9290/

pelvic region (Sakthivelavan et al., 2014). The objective of this study was to analyse the influence of these small branching arteries on the haemodynamics and physical flow phenomena commonly associated with aneurysmal disease: specifically regions of low and oscillatory wall shear stress (WSS). As this work forms a first look into modelling the iliac arteries and their branches, an understanding of these minor arteries must be established, and the role they play in the prediction of disease throughout the remainder of the iliac artery, notably in the common and internal iliac arteries (the iliac arteries most susceptible to aneurysmal development). The haemodynamics within the internal iliac artery is expected to be altered by the presence of local minor arteries, while the common iliac artery is likely too far upstream. This investigation also provides an opportunity to comment on the omission of minor arteries from other large artery CFD models – where little to no justification has been provided.

2. Methods

2.1. Patient-specific geometry

We reconstructed the aorta and branching arteries from the CT dataset of a 91-year-old male patient with a CIAA, with distal extension to the bifurcation of the internal and external iliac arteries. The typical healthy common iliac artery bifurcates into the internal and external iliac arteries, where the former is often smaller in diameter than the latter. The internal iliac artery divides variably into approximately 10 smaller branches (see Fig. 1).

Contrast-enhanced CT data (pixel size=0.82 mm; slice thickness=1 mm) was imported into Mimics v17 (Materialise, Belgium). The lumen was reconstructed into 3D using a pixel intensity-based thresholding approach and the resulting surfaces were conservatively smoothed, following previous methods (Doyle et al., 2007; Doyle et al., 2014a, 2014b). We created two geometries; one full geometry with the branching arteries (five artery outlets branching from the right internal iliac artery and three outlets from the left internal iliac artery), and another where we manually trimmed all branching arteries from the internal iliac arteries (see Fig. 2). All outlets were cut orthogonal to the centreline and we extended each outlet by 10 times the outlet diameter so that outlet boundary conditions would not affect haemodynamics within the vessel. We also extended the inlet section by 120 mm based on the unsteady entrance length method suggested by Wood (1999), to ensure flow was fully developed entering the supraceliac (SC) aorta. This extension was created by extruding the inlet surface.

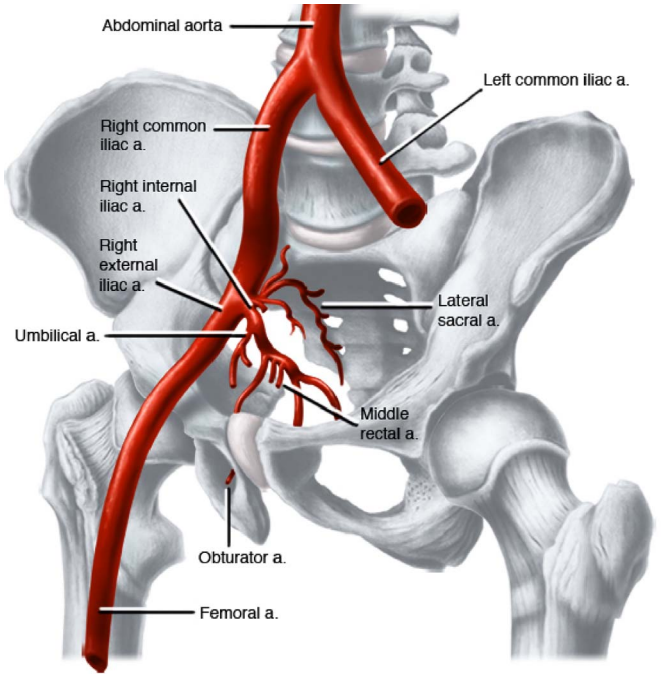

Fig. 1. Normal anatomy of the iliac artery region showing the multiple branches from the internal iliac artery (Fitzgerald, 2015).

2.2. Computational mesh

The volume mesh was constructed within STAR-CCM+ (v9.04) (CD-adapco Group) using a core (unstructured) polyhedral mesh and a prism-layer mesh near the wall boundary. The prism-layer mesh was progressively refined approaching the wall. The thickness of the prism-layer mesh and the surface size (edge length) were defined relative to the local lumen diameter so that the minor arteries were well discretised. Any areas that were expected to have rapid changes in velocity (i.e. bifurcations) were also subject to refinement (see Fig. 3b). The polyhedral mesh was chosen over the more common tetrahedral mesh as they offer (finite-volume) solutions of similar accuracy at lower cost: in haemodynamic simulations of cerebral aneurysms, polyhedral meshes required a quarter the number of tetrahedral cells to obtain similar converged values of WSS (Spiegel et al., 2011).

In order to determine a sufficient level of (uniform) mesh refinement, the Grid Convergence Index (GCI) (Celik et al., 2008; Roache, 1994) was calculated from the results of a steady-state simulation using the peak systolic flow conditions (see Fig. 3a). The GCI was determined for WSS in the aneurysm region, the pressure at the inlet and the velocity throughout the geometry using scattered probes. We deemed the mesh optimal when the GCI $<$ 2% (Doyle et al., 2014a).

2.3. Physical assumptions and boundary conditions

The blood flow was approximated as laminar and was considered to be an isothermal, incompressible, Newtonian fluid with a dynamic viscosity of 0.0035 Pa s and a density of 1050 kg/m^3. The walls of the arteries were characterised by no-slip, rigid wall boundary conditions (Boyd et al., 2015; Doyle et al., 2014a; Les et al., 2010a, 2010b; Poelma et al., 2015; Steinman et al., 2013) and the Navier–Stokes (and continuity) equations were solved using STAR-CCM+. The temporal discretisation was second order, with 10^3 steps per cardiac cycle and 15 inner iterations: the convergence of both the continuity and momentum residuals remained below 10^{-3} throughout the cardiac cycle. A scaled mass flow waveform was applied at the supraceliac (SC) inlet based on the volumetric flow data and age-estimated fat-free body mass scaling law of Les et al. (2010a, 2010b) (see Fig. 3a). During the peak of the systolic and diastolic phases, the flow through each common iliac artery was 55 ml/s and −7 ml/s (back flow), respectively.

The model explicitly coupled the 3D CFD simulation with a three-element Windkessel model at each outlet boundary in order to approximate the resistance and compliance of the downstream vascular beds. The Windkessel parameters are calibrated according to previous methodology (Laskey et al., 1990; Les et al., 2010a, 2010b); with 30% of the common iliac flow passing through to the internal iliac artery. The flow leaving each internal iliac artery outlet was directly proportional to its mean cross-sectional area.

2.4. Data analysis

The solutions to each of the geometries were compared for the time average WSS (TAWSS), oscillatory shear index (OSI) (Ku et al., 1985) and time-averaged velocity profiles. When comparing the solutions of the two geometries ('original' and 'trimmed') the changes in the TAWSS, the OSI, and the time-averaged velocity profiles (upstream of the trimming locations) were investigated. The discrete calculation of these variables was done for 100 intervals per cardiac cycle, and once the boundary waveforms converged (and any initial transience was not present) the results were calculated for 10 cardiac cycles. Averaging for 10 cardiac cycles is traditionally quite conservative, with many studies taking these fields over three or five cycles (Di Achille et al., 2014; Doyle et al., 2014a; Les et al., 2010a, 2010b). However, in light of a recent study by Poelma et al. (2015), the statistical convergence of these variables was investigated; Poelma et al. showed a similar case where averaging 28 cycles of data did not lead to the complete convergence of OSI at a particular location.

3. Results

3.1. Grid and cycle convergence

All tested variables for the GCI returned values below 2%. As this is considered to be a sufficient minimisation of the spatial discretisation error, no further mesh refinement was performed.

Please cite this article as: Kelsey, L.J., et al., The influence of downstream branching arteries on upstream haemodynamics. Journal of Biomechanics (2016), http://dx.doi.org/10.1016/j.jbiomech.2016.07.023

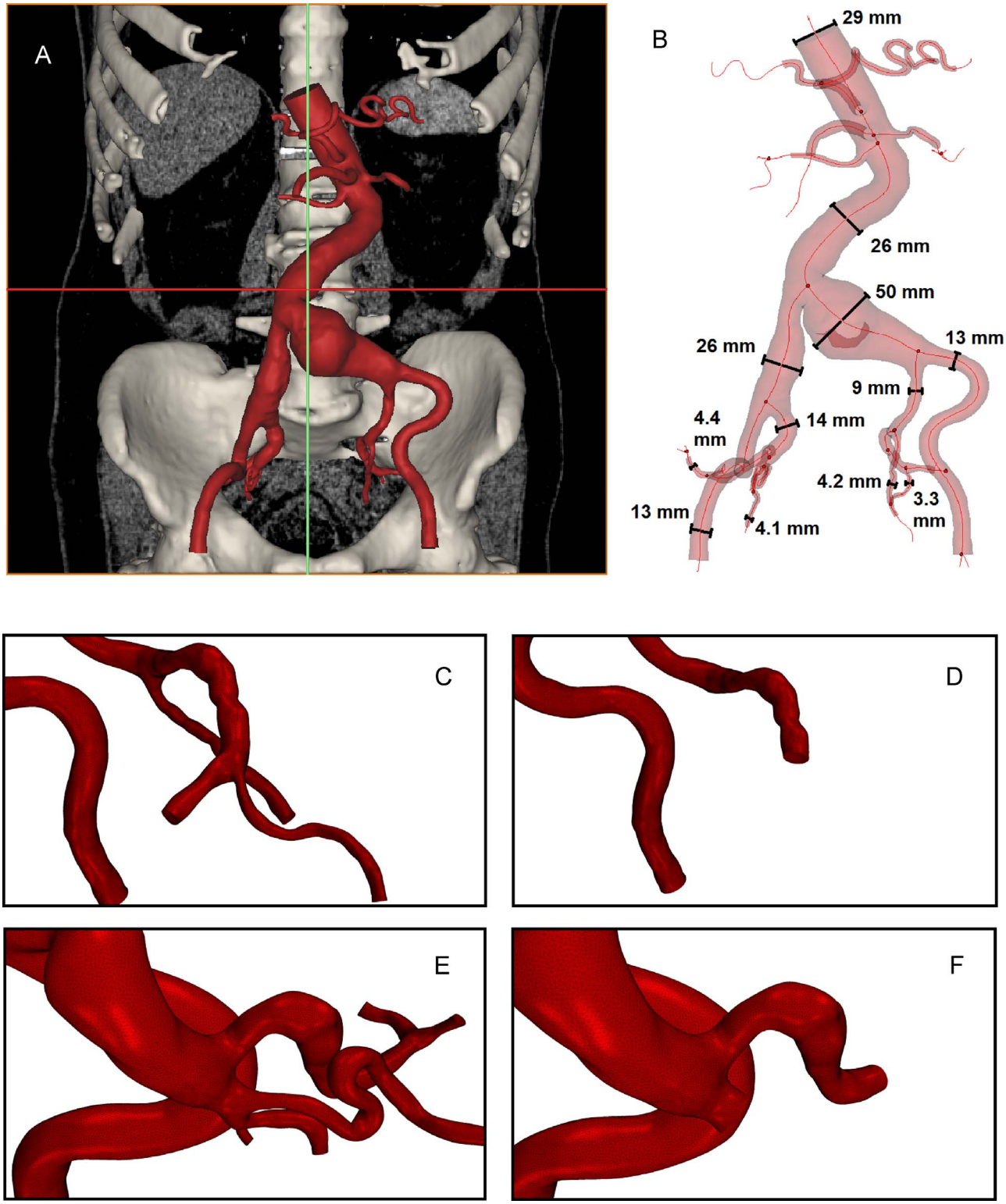

Fig. 2. (A) 3D reconstruction from CT showing the patient's artery lumen. (B) Transparent reconstruction showing the artery centrelines and diameters. (C) Right internal iliac artery (IIA) region before trimming and (D) after trimming. (E) Left IIA region before trimming and (F) after trimming.

The resulting meshes contained 16 prism-layers and total mesh-cell counts of approximately 5.8 and 4.8 million for the original and trimmed geometries, respectively. When compared to Poelma et al. (2015), the convergence of results was not so slow and a 10 cardiac cycle averaging was sufficient. The mean relative error between a 10-cycle average and a nine-cycle average was 0.2% for TAWSS and 0.5% for OSI across the large CIAA.

3.2. *Influence of branching arteries*

The TAWSS is very similar for both geometries (see Fig. 4). The only clear differences are in (and downstream from) the regions where the branching arteries were trimmed. Fig. 4 shows just how localised the change is to these regions. The red areas in Fig. 4c show the regions of 10% change or more, while the histograms

Please cite this article as: Kelsey, L.J., et al., The influence of downstream branching arteries on upstream haemodynamics. Journal of Biomechanics (2016), http://dx.doi.org/10.1016/j.jbiomech.2016.07.023

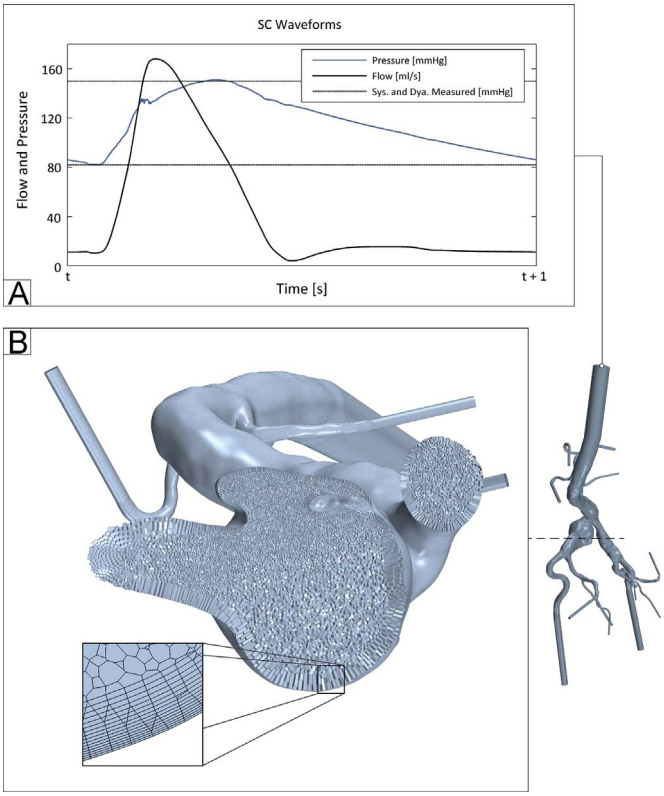

Fig. 3. (A) SC inlet waveforms and the patient's systolic and diastolic blood pressures. (B) Mesh cross-section through the CIAA 'pocket', highlighting the prism-layer mesh and local mesh refinement.

show the area-weighted variation of the relative error for the four surfaces shown. The mean change across these surfaces is approximately 2%, and any large variations in these upstream locations are slight misalignments between patches of TAWSS. Similar trends were observed for the OSI: the mean relative error for all the surfaces is less than 5%. The predominant variation between the two solutions is again around, or downstream of the trimmed arteries – where the OSI changes by more than 20% for the majority of cell faces.

OSI ranges from 0 to 0.5 and based on the work of Ku et al. (1985), OSI $>$ 0.3 can be considered as high, and detrimental, due to the occurrence of intimal thickening and atherosclerotic plaques in regions of OSI above this threshold. Here we observed 10.2% of the original geometry surface area local-to and downstream-from the minor arteries (in the internal iliac arteries) to be above 0.3, compared to 8.3% in the trimmed geometry; where, 5.7% of this surface contained high OSI regions common to both geometries (i.e. overlapped). In relation to TAWSS, previous work has shown that leucocyte adhesion exponentially increases as TAWSS drops below 0.36 Pa and approaches zero (Lawrence et al., 1995; Lawrence et al., 1987; Worthen et al., 1987). This threshold was subsequently included into computational studies as a way to associate regions of low TAWSS with particle residence and deposition (Hardman et al., 2013). It is employed here as a marker of low wall shear stress (which should be considered alongside other haemoydynamic indicators). In our original geometry, 32.5% of the surface area local-to or downstream-from the minor arteries is below this threshold, compared to only 12.7% in the trimmed geometry; where 11.5% of this surface contained low TAWSS regions common to both geometries. The original geometry has a considerably lower TAWSS in internal iliac arteries as a significant portion of the flow is shared with the branching arteries, reducing the velocity in the downstream of the parent vessel.

The velocity field was compared at cross-sections within the common and internal iliac arteries. Fig. 5 shows the time-averaged velocity magnitude profiles within the patient's aneurysm, examining the velocity in and around the 'pocket' where the flow is complex. There is very little change between the velocity magnitude profiles at this location. Negligible change was also observed the other measurement locations (upstream of the trimming locations) (Fig. 5).

4. Discussion

When imaging abdominal aortic aneurysms or iliac artery aneurysms with routine CT parameters, the smaller branching arteries of the internal iliac artery are often not captured. Therefore, in resulting 3D reconstructions, the branches are omitted. It is clear that trimming the minor downstream arteries results in a negligible change to the upstream haemodynamics. However, the flow-field where the minor arteries were trimmed is different, as expected, and near the trimming locations the TAWSS and OSI varies by more than 10% and 20%, respectively changing the interpretation of the analysed haemodynamic disease-indicators.

Similar observations were made in the carotid artery (Zhao et al., 1999) and may occur when trimming minor arteries from other large artery regions. Fortunately for the common iliac arteries, as there are no small arteries branching from them, simply the presence of the external-internal iliac bifurcation may be sufficient to minimise the effect that the downstream arteries

Please cite this article as: Kelsey, L.J., et al., The influence of downstream branching arteries on upstream haemodynamics. Journal of Biomechanics (2016), http://dx.doi.org/10.1016/j.jbiomech.2016.07.023

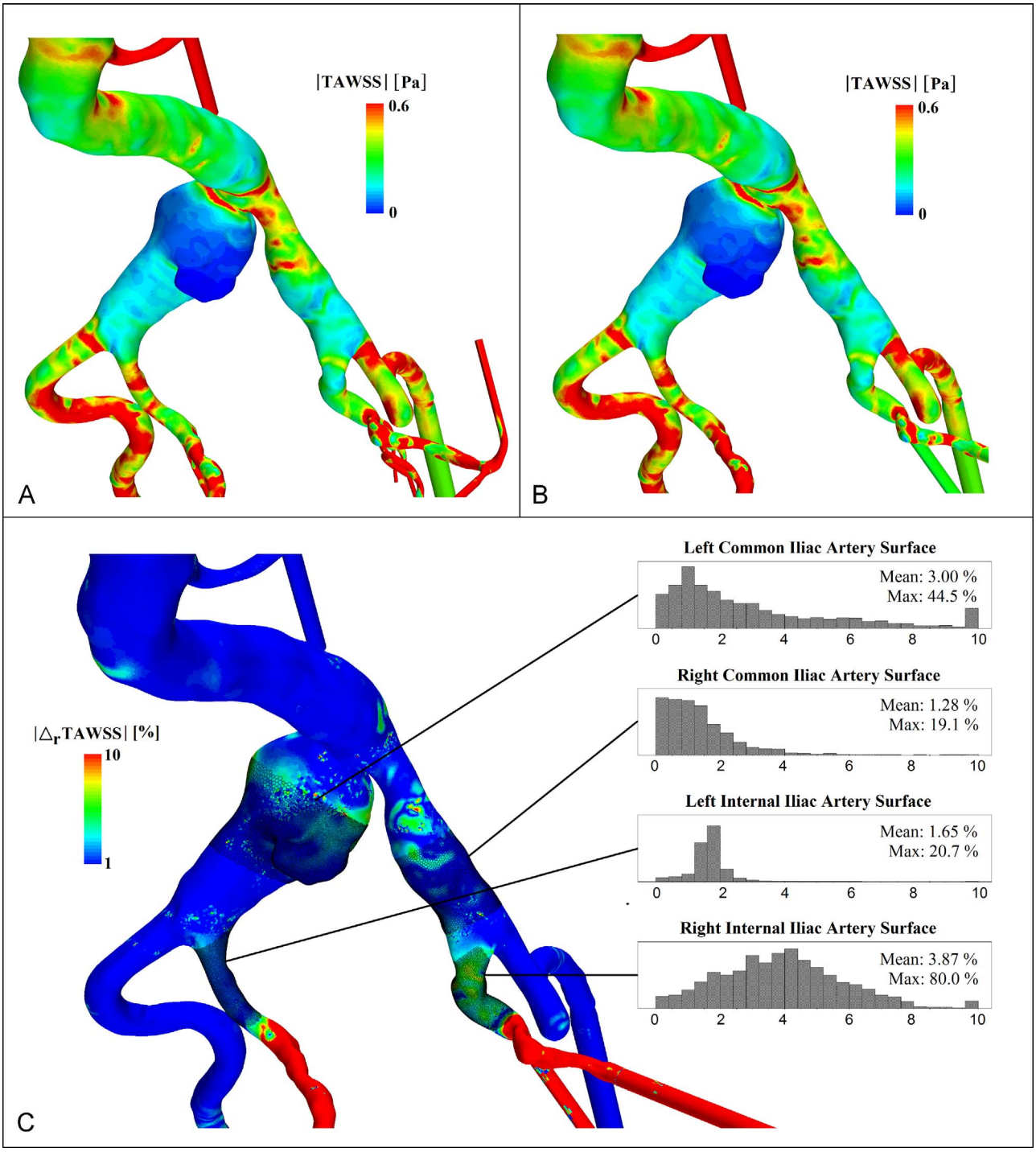

Fig. 4. (A) TAWSS field for the original (untrimmed) geometry. (B) TAWSS field for trimmed geometry. (C) The relative error between the TAWSS field computed for the original (untrimmed) geometry and the trimmed geometry. The histograms on the right-hand side show the area-weighted distribution of this error for the four surfaces shown.

have on the computed flow-field within them. However, it is recommended that care be taken when analysing haemodynamic data obtained from models of internal iliac artery aneurysms that omit local minor-branching arteries.

It should be noted that the results of this study would be more substantive if more geometries were available for consideration. The configuration and reconstruction of the minor arteries would alter the boundary conditions, required temporal averaging and results. However, a similar outcome would be expected.

5. Conclusion

The omission of smaller branching downstream arteries has a negligible qualitative or quantitative impact on upstream haemodynamics. This present work supports the omission of smaller iliac

Please cite this article as: Kelsey, L.J., et al., The influence of downstream branching arteries on upstream haemodynamics. Journal of Biomechanics (2016), http://dx.doi.org/10.1016/j.jbiomech.2016.07.023

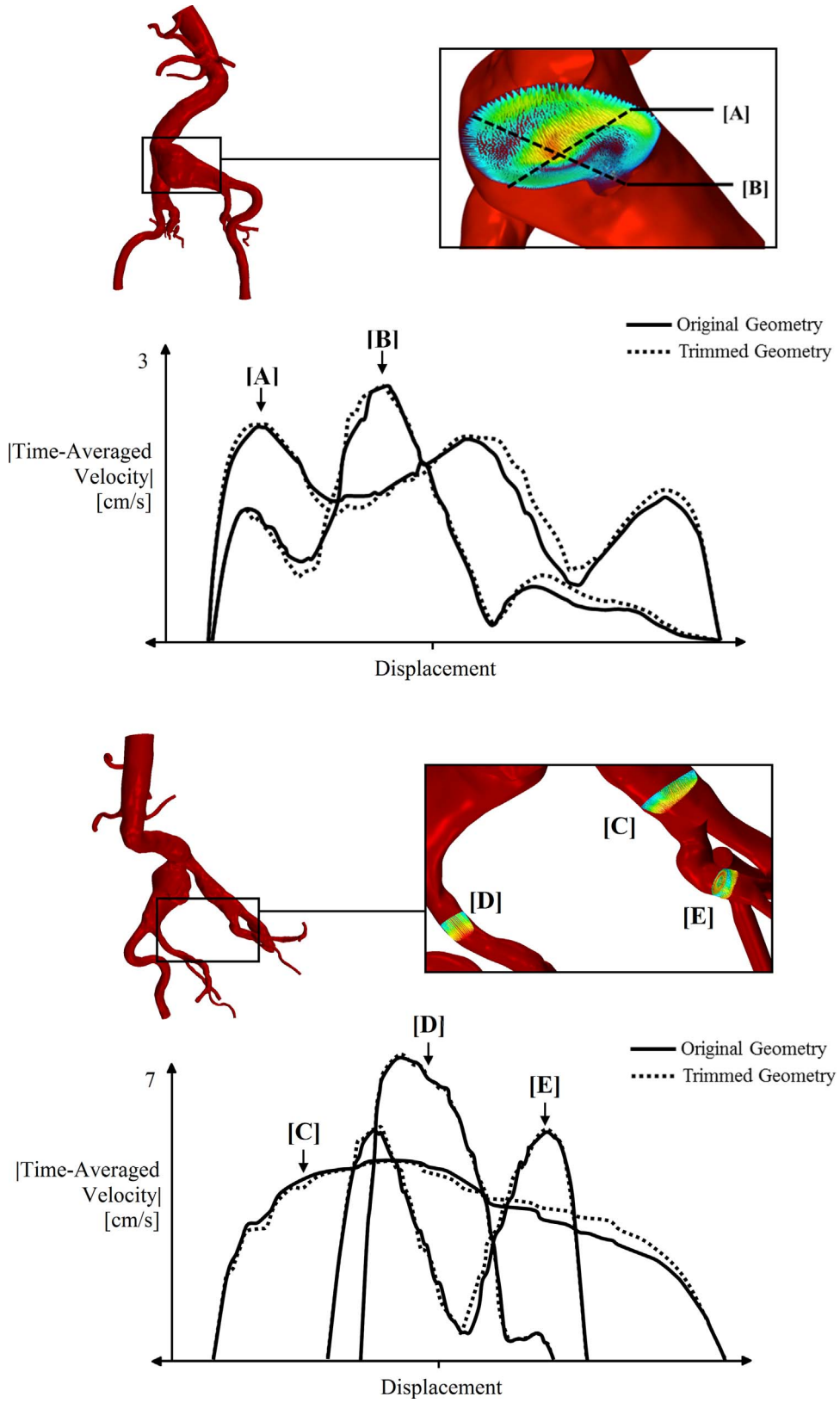

Fig. 5. Time-averaged velocity magnitude profiles in the CIAA (top). These profiles are plotted along the lines [A] and [B] to compare the solution to velocity within the aneurysm for the original and trimmed geometries. A comparison of the time-averaged velocity magnitude profiles in the other common iliac ([C]) and internal iliac arteries ([D], [E]) upstream of the trimming locations (bottom).

Please cite this article as: Kelsey, L.J., et al., The influence of downstream branching arteries on upstream haemodynamics. Journal of Biomechanics (2016), http://dx.doi.org/10.1016/j.jbiomech.2016.07.023

artery branches in previous CFD studies involving the aortic bifurcation.

Funding

We would like to thank the National Health and Medical Research Council, Australia (Grants APP1063986 and APP1083572), the Australian Postgraduate Award, and the Intelligent Systems for Medicine Laboratory Computational Biomechanics for Medicine Scholarship.

Conflicts of interest

No conflicts of interest.

Acknowledgements

The authors would like to thank CD-adapco for their support of our research.

References

Blacher, J., Asmar, R., Djane, S., London, G.M., Safar, M.E., 1999. Aortic pulse wave velocity as a marker of cardiovascular risk in hypertensive patients. Hypertension 33, 1111–1117. http://dx.doi.org/10.1161/01.hyp.33.5.1111.

Boyd, A.J., Kuhn, D.C., Lozowy, R.J., Kulbisky, G.P., 2015. Low wall shear stress predominates at sites of abdominal aortic aneurysm rupture. J. Vasc. Surg. 63, 1613–1619. http://dx.doi.org/10.1016/j.jvs.2015.01.040.

Celik, I.B., Ghia, U., Roache, P.J., Freitas, C.J., Coleman, H., Raad, P.E., 2008. Procedure for estimation and reporting of uncertainty due to discretization in CFD applications. J. Fluids Eng. 130, 1–4.

Di Achille, P., Tellides, G., Figueroa, C.A., Humphrey, J.D., 2014. A haemodynamic predictor of intraluminal thrombus formation in abdominal aortic aneurysms. Proc. R. Soc. A: Math., Phys. Eng. Sci. 470, 20140163. http://dx.doi.org/10.1098/rspa.2014.0163.

Doyle, B., Callanan, A., McGloughlin, T., 2007. A comparison of modelling techniques for computing wall stress in abdominal aortic aneurysms. Biomed. Eng. Online, 6. http://dx.doi.org/10.1186/1475-925X-6-38.

Doyle, B.J., Callanan, A., Burke, P.E., Grace, P.A., Walsh, M.T., Vorp, D.A., et al., 2009. Vessel asymmetry as an additional diagnostic tool in the assessment of abdominal aortic aneurysms. J. Vasc. Surg. 49, 443–454. http://dx.doi.org/10.1016/j.jvs.2008.08.064.

Doyle, B.J., McGloughlin, T.M., Kavanagh, E.G., Hoskins, P.R., 2014a. From detection to rupture: a serial computational fluid dynamics case study of a rapidly expanding, patient-specific, ruptured abdominal aortic aneurysm. In: Doyle, B., Miller, K., Wittek, A., Nielsen, M.F.P. (Eds.), Computational Biomechanics for Medicine: Fundamental Science and Patient-specific Applications. Springer, New York, pp. 53–68. http://dx.doi.org/10.1007/978-1-4939-0745-8_5.

Doyle, B.J., McGloughlin, T.M., Miller, K., Powell, J.T., Norman, P.E., 2014b. Regions of high wall stress can predict the future location of rupture of abdominal aortic aneurysm. Cardiovasc. Interv. Radiol. 37, 815–818. http://dx.doi.org/10.1007/s00270-014-0864-7.

Human Gross Anatomy Atlas. Available from: ⟨http://cias.rit.edu/~tpf1471/Fitzgerald_783/anatomy/pelvisSkeleton.html⟩. [1 May 2015].

Gasser, T.C., Auer, M., Labruto, F., Swedenborg, J., Roy, J., 2010. Biomechanical rupture risk assessment of abdominal aortic aneurysms: model complexity versus predictability of finite element simulations. Eur. J. Vasc. Endovasc. Surg. 40, 176–185. http://dx.doi.org/10.1016/j.ejvs.2010.04.003.

Hardman, D., Doyle, B.J., Semple, S.I., Richards, J.M., Newby, D.E., Easson, W.J., et al., 2013. On the prediction of monocyte deposition in abdominal aortic aneurysms using computational fluid dynamics. Proc. Inst. Mech. Eng., 1114–1124. http://dx.doi.org/10.1177/0954411913494319.

Huang, Y., Gloviczki, P., Duncan, A.A., Kalra, M., Hoskin, T.L., Oderich, G.S., et al., 2008. Common iliac artery aneurysm: expansion rate and results of open surgical and endovascular repair. J. Vasc. Surg. 47, 1203–1210. http://dx.doi.org/10.1016/j.jvs.2008.01.050.

Ku, D.N., Giddens, D.P., Zarins, C.K., Glagov, S., 1985. Pulsatile flow and atherosclerosis in the human carotid bifurcation. Positive correlation between plaque location and low oscillating shear stress. Arter. Thromb. Vasc. Biol. 5, 293–302. http://dx.doi.org/10.1161/01.atv.5.3.293.

Laskey, W.K., Parker, H.G., Ferrari, V.A., Kussmaul, W.G., Noordergraaf, A., 1990. Estimation of total systemic arterial compliance in humans. J. Appl. Physiol. 69, 112–119.

Lawrence, M.B., Berg, E.L., Butcher, E.C., Springer, T.A., 1995. Rolling of lymphocytes and neutrophils on peripheral node addressin and subsequent arrest on ICAM-1 in shear flow. Eur. J. Immunol. 25, 1025–1031. http://dx.doi.org/10.1002/eji.1830250425.

Lawrence, M.B., McIntire, L.V., Eskin, S.G., 1987. Effect of flow on polymorphonuclear leukocyte/endothelial cell adhesion. Blood 70, 1284–1290.

Les, A.S., Shadden, S.C., Figueroa, C.A., Park, J.M., Tedesco, M.M., Herfkens, R.J., et al., 2010a. Quantification of hemodynamics in abdominal aortic aneurysms during rest and exercise using magnetic resonance imaging and computational fluid dynamics. Ann. Biomed. Eng. 38, 1288–1313. http://dx.doi.org/10.1007/s10439-010-9949-x.

Les, A.S., Yeung, J.J., Schultz, G.M., Herfkens, R.J., Dalman, R.L., Taylor, C.A., 2010b. Supraceliac and infrarenal aortic flow in patients with abdominal aortic aneurysms: mean flows, waveforms, and allometric scaling relationships. Cardiovasc. Eng. Technol. 1, 39–51. http://dx.doi.org/10.1007/s13239-010-0004-8.

Norman, P.E., Lawrence-Brown, M., Semmens, J., Mai, Q., 2003. The anatomical distribution of iliac aneurysms: is there an embryological basis? Eur. J. Vasc. Endovasc. Surg. 25, 82–84. http://dx.doi.org/10.1053/ejvs.2002.1780.

Pijls, N.H.J., de Bruyne, B., Peels, K., van der Voort, P.H., Bonnier, H.J.R.M., Bartunek, J., et al., 1996. Measurement of fractional flow reserve to assess the functional severity of coronary-artery stenoses. New Engl. J. Med. 334, 1703–1708. http://dx.doi.org/10.1056/NEJM199606273342604.

Poelma, C., Watton, P.N., Ventikos, Y., 2015. Transitional flow in aneurysms and the computation of haemodynamic parameters. J. R. Soc. Interface 12, 20141394. http://dx.doi.org/10.1098/rsif.2014.1394.

Roache, P.J., 1994. Perspective: a method for uniform reporting of grid refinement studies. J. Fluids Eng. 116, 405–413.

Sakthivelavan, S., Aristotle, S., Sivanandan, A., Sendiladibban, S., Jebakani, C.F., 2014. Variability in the branching pattern of the internal iliac artery in indian population and its clinical importance. Anat. Res. Int. 2014, 1–6. http://dx.doi.org/10.1155/2014/597103.

Spiegel, M., Redel, T., Zhang, Y.J., Struffert, T., Hornegger, J., Grossman, R.G., et al., 2011. Tetrahedral vs. polyhedral mesh size evaluation on flow velocity and wall shear stress for cerebral hemodynamic simulation. Comput. Methods Biomech. Biomed. Eng. 14, 9–22. http://dx.doi.org/10.1080/10255842.2010.518565.

Steinman D.A., Hoi Y., Fahy P., Morris L., Walsh M.T., Aristokleous N., et al., 2013. Variability of computational fluid dynamics solutions for pressure and flow in a giant aneurysm. In: The proceedings of the ASME 2012 Summer Bioengineering Conference CFD Challenge. Journal of Biomechanical Engineering 135, 021016. 10.1115/1.4023382.

Sun, Z., Xu, L., 2014. Computational fluid dynamics in coronary artery disease. Comput. Med. Imaging Graph. 38, 651–663. http://dx.doi.org/10.1016/j.compmedimag.2014.09.002.

Svensjö, S., Björck, M., Gürtelschmid, M., Djavani Gidlund, K., Hellberg, A., Wanhainen, A., 2011. Low prevalence of abdominal aortic aneurysm among 65-year-old swedish men indicates a change in the epidemiology of the disease. Circulation 124, 1118–1123. http://dx.doi.org/10.1161/circulationaha.111.030379.

Tendera, M., Aboyans, V., Bartelink, M.-L., Baumgartner, I., Clément, D., Collet, J.-P., et al., 2011. ESC Guidelines on the diagnosis and treatment of peripheral artery diseases. Document covering atherosclerotic disease of extracranial carotid and vertebral, mesenteric, renal, upper and lower extremity arteries. Task. Force Diagn. Treat. Peripher. Artery Dis. Eur. Soc. Cardiol. (ESC) 32, 2851–2906. http://dx.doi.org/10.1093/eurheartj/ehr211.

Tonino, P.A.L., De Bruyne, B., Pijls, N.H.J., Siebert, U., Ikeno, F., van `t Veer, M., et al., 2009. Fractional flow reserve versus angiography for guiding percutaneous coronary intervention. New Engl. J. Med. 360, 213–224. http://dx.doi.org/10.1056/NEJMoa0807611.

Wilkinson, I.B., Cockcroft, J.R., Webb, D.J., 1998. Pulse wave analysis and arterial stiffness. J. Cardiovasc. Pharmacol. 32 (Suppl 3), S33–S37.

Wood, N.B., 1999. Aspects of fluid dynamics applied to the larger arteries. J. Theor. Biol. 199, 137–161. http://dx.doi.org/10.1006/jtbi.1999.0953.

Worthen, G.S., Smedly, L.A., Tonnesen, M.G., Ellis, D., Voelkel, N.F., Reeves, J.T., et al., 1987. Effects of shear stress on adhesive interaction between neutrophils and cultured endothelial cells. J. Appl. Physiol. (Bethesda, Md. : 1985) 63, 2031–2041.

Zhao, S.Z., Xu, X.Y., Collins, M.W., Stanton, A.V., Hughes, A.D., Thom, S.A., 1999. Flow in carotid bifurcations: effect of the superior thyroid artery. Med. Eng. Phys. 21, 207–214, S1350-4533(99)00046-6 [pii].

Please cite this article as: Kelsey, L.J., et al., The influence of downstream branching arteries on upstream haemodynamics. Journal of Biomechanics (2016), http://dx.doi.org/10.1016/j.jbiomech.2016.07.023